ELSEVIER

Journal of Nuclear Materials 302 (2002) 73–88

journal of nuclear materials

www.elsevier.com/locate/jnucmat

Review

Present limits and improvements of structural materials for fusion reactors – a review

A.-A.F. Tavassoli *

DMN/Dir, DEN, CEA Saclay, 91191 Gif-sur-Yvette cedex, France

Received 16 November 2001; accepted 31 January 2002

Abstract

Since the transition from ITER or DEMO to a commercial power reactor would involve a significant change in system and materials options, a parallel R&D path has been put in place in Europe to address these issues. This paper assesses the structural materials part of this program along with the latest R&D results from the main programs. It is shown that stainless steels and ferritic/martensitic steels, retained for ITER and DEMO, will also remain the principal contenders for the future FPR, despite uncertainties over irradiation induced embrittlement at low temperatures and consequences of high He/dpa ratio. Neither one of the present advanced high temperature materials has to this date the structural integrity reliability needed for application in critical components. This situation is unlikely to change with the materials R&D alone and has to be mitigated in close collaboration with blanket system design. © 2002 Published by Elsevier Science B.V.

1. Introduction

The development of structural materials for fission reactors has followed an evolutionary path, constantly building upon the experience acquired from previous generations. The structural materials development for the fusion power reactors (FPR) can also benefit from the fission experience but in several cases, notably for magnets, vessel and in vessel components, must rely on its own evolutionary path. This will be achieved through construction of ITER, testing of blanket modules in ITER and development of a demonstration reactor (DEMO). However, since the transition from ITER or DEMO to a commercial power reactor would involve a significant change in system and material options, the European R&D program also includes a parallel path that investigates more advanced materials, as well as provisions for an intense neutron source facility (IFMIF) for testing all candidate materials. Other partners have similar programs, with US putting their main emphasis on materials for high performance fusion power systems, e.g. advanced power extraction (APEX) project [1,2].

The primary objective of this paper is to assess materials requirements for the fusion power reactor. For this purpose, the latest information on the structural materials from the ongoing investigations are collected and assessed in terms of strength, embrittlement and efficiency. From the conclusions drawn and in conjunction with the results that are expected to become available at the end of the currently implemented programs, suggestions are formulated for improvement of the European structural materials programs [3].

2. Materials

A wide range of structural materials is already being investigated for ITER [4–6] and DEMO [7–10]. The list includes conventional materials (e.g., austenitic stainless steels, copper alloys, titanium alloys, chromium alloys and nickel base alloys), low-activation structural materials (ferritic–martensitic steels including ODS, vanadium alloys, and ceramic composites), as well as materials for high heat flux regions (e.g. tungsten and CFC).

* Tel.: +33-1 69 08 60 21; fax: +33-1 69 08 80 70.
E-mail address: tavassoli@cea.fr (A.-A.F. Tavassoli).

0022-3115/02/$ - see front matter © 2002 Published by Elsevier Science B.V.
PII: S0022-3115(02)00794-8

Table 1
Common structural materials with examples of their applications

Category	Example of materials	Present or projected application examples
Aluminum alloys	2014, 2024, 6061	Pool type reactor vessels, aeronautics
Copper alloys	CuCrZr, DS-Cu	ITER heat sink and divertor
Titanium alloys	Ti–6Al–4V	ITER and aeronautics
F/M steels	F82H, JLF, Eurofer	ITBM, DEMO
ODS steels	Fe–Y_2O_3	FBR, fusion
Stainless steels	316, 304, 321	ITER, LWR and LMFBR
Nickel base alloys	In. 718, 625, 623	ITER, HTGR
Superalloys	Hastalloys, Haynes series	Aerospace, space reactors
Vanadium alloys	V–4Cr–4Ti	DEMO, FPR
Molybdenum alloys	Mo, TZM, Mo–Re	Aerospace and space reactors
Niobium alloys	Cb275, FS85, Nb–1% Zr	Aerospace, nuclear industry
Tantalum alloys	Ta–8W–2Hf	Space reactors
Tungsten alloys	W, W–Re, W–ThO_2	ITER
Ceramic composites	SiC_f/SiC, CFC	Fusion and aeronautics

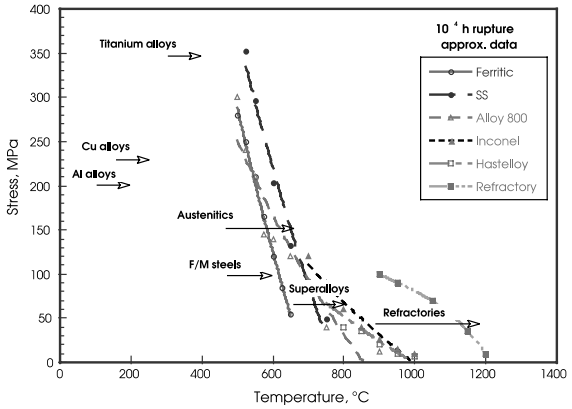

Fig. 1. Approximate upper temperature limit of structural materials based on 10^4 h creep-rupture time [11].

More recently, high temperature refractory metal alloys (Cr, Nb, Ta, Mo and W alloys) have been added to the list of structural materials [1–3], because they offer higher temperature capabilities and that their eventual higher nuclear activation may be offset by a more compact design [2]. Table 1 presents an overview of the common structural materials, categorized in the order of their increasing maximum service temperature. Fig. 1 uses the 10 000 h thermal creep rupture data of some of these materials to visualize approximate upper service temperatures of each category [11].

Obviously, an assessment of all these materials in this paper is unrealistic. Instead, our attention will be focused on high temperature materials for first wall and blanket components: stainless steels, F/M steels, ODS steels, ceramic composites and refractory metal alloys.

3. Selection criteria

It is difficult to discuss selection criteria for structural materials without including the overall system parameters: tritium breeding material, coolant medium, neutron multiplier, plasma facing material, tritium barrier, insulation, etc. Often these parameters impact the acceptability and performance limits of candidate materials or limit their service temperature window. Table 2 presents some of these parameters for the leading structural materials. Obviously these parameters are tentative and not necessarily representative of the final system that will be selected for the future FPR in the next 50–100 years. Already other cooling media (such as Sn–Li, Li_2BF_4) and systems (inertial, free surface liquid walls, etc.) are put forward [1,2,7].

It is also difficult to discuss selection criteria without including the availability and cost of materials. Indeed, while small differences in cost of materials is negligible compared to the cost of one-day reactor stoppage, the cost of materials such as SiC_f/SiC and some refractory metal alloys (Ta and W) are several magnitudes higher than conventional steels. Likewise, the selection criteria should include joining, inspection, or how materials will be produced and in what shape or form they will be used. For instance, one cannot use wrought material properties data for a material that will be cast or HIPed when put in service.

More important yet, one has to recognize that the selection of materials for application in the nuclear industry must include a high safety margin, and rely on high quality materials data, often backed by service experience. In fact, past experience shows that the complexity of the service conditions in nuclear reactors is such that laboratory tests may not reproduce the full extent of damage.

Table 2
Primary candidate materials considered for the first wall blanket system of fusion power system

Structural materials	Tritium breeding materials	Coolant	Neutron multiplier	Plasma facing materials	Other materials
Vanadium alloys	Lithium	Li	Be	Be	T-barrier
F/M steels	Pb–Li (WCLL)	H_2O	Pb	Be, C	Insulator
	Li_4SiO_4 (HCPB)	He	Be	Be, C	
SiC_f/SiC	Pb–Li (Tauro)	Pb–Li	Pb–Li	W	Insulating

While recognizing the importance of all the above considerations in this paper, we shall use the available data, not to make a critical assessment, but a rough assessment of the candidate materials for a better definition of future R&D work. Even then, we do recognize the disparity amongst the quantity and quality of data available for each material. We ignore at this stage new proposed structural integrity design rules, either to take into account low uniform elongation values (e.g. using the allowable total stress intensity S_d instead of $3S_m$ to calculate surface heat flux) [1] or to integrate material heterogeneity (new calculation methodologies for SiC_f/SiC) [10].

Each assessment chapter will include the following topics:

1. General description of materials.
2. Tensile properties: Tension test results will be used for calculating the allowable primary membrane stress intensity S_m. When the information is not available for an accurate calculation of S_m, a third of the minimum ultimate tensile strength will be taken to be equal to S_m.
3. Creep properties: Isothermal creep test results will be used for calculating the allowable time dependent stress intensity S_t. When the available information is insufficient, 2/3 of the minimum stress to rupture will be used to derive S_t.
4. Fatigue properties: low cycle strain controlled fatigue test results will be used for calculating fatigue design curves.
5. Surface heat capability: physical properties (Young's modulus (E), coefficient of linear thermal expansion (α_i) and thermal conductivity (k)) and S_m will be used to estimate a figure of merit of surface heat capability for each material. $Qw \approx M = 3S_m k(1-\nu)/(\alpha_i E)$, where ν is Poisson's ratio, Q the maximum allowable heat flux and w wall thickness.
6. Embrittlement: post-irradiation test results will be used to assess embrittlement at low and high temperatures.
7. Future perspectives: at the end of each assessment, temperature window, compatibility issues and future perspectives for each material will be briefly discussed.

4. Materials properties

4.1. Austenitic stainless steels

4.1.1. General description

Several grades of this steel (316, 304, 321, etc.) are fully code qualified and have been extensively used in the nuclear industry over the past 30 years. We shall use the data from the Appendix A of IISDC (ITER Interim Structural Design Criteria) and RCC-MR for Type 316LN, i.e. the ITER Grade (IG) selected for ITER (316LN-IG), in the following analysis (see Ref. [12], and updated results in the Appendix A of the ITER Structural Design Code, ITER Team).

4.1.2. Tensile properties

Fig. 2 shows variations of ultimate and yield tensile strengths of 316LN versus test temperature. The large difference between yield strength and UTS is an indication of materials high toughness, but in turn the lower YS governs S_m values. As shown in Fig. 2, the strength of the type 316LN decreases at temperatures higher than 600 °C and this steel is seldom used above 700 °C.

4.1.3. Creep properties

Type 316LN-IG has a superior creep resistance to steels such as types 304L and 316L [12]. At 550 °C, stresses to cause rupture in 1000, 10 000 and 1 00 000 h are of the order of 248, 195 and 150 MPa, respectively.

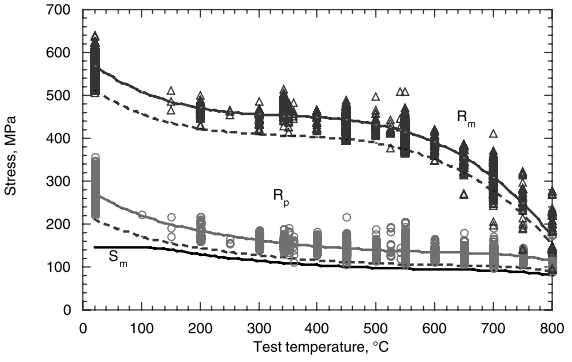

Fig. 2. Tensile properties of 316LN versus temperature used for calculating S_m [12].

4.1.4. Fatigue properties

Fatigue properties of type 316LN are well documented. The average total strain amplitude (half strain range) for 10 000 continuous fatigue cycling is about 0.30% (design value of 0.15).

Significant cyclic hardening occurs in 316LN steel during the first few cycles, the amount of which depends on the applied strain. For a total strain amplitude of about 0.25%, the stress amplitude is raised by about 225 MPa.

4.1.5. Surface heat capability

Physical properties of 316LN at several temperatures are shown in Table 3. The surface heat capability factor (M) derived from these values is also shown in the table. As it can be seen, these values are low and for a wall thickness of about 2 mm, the maximum heat flux would be limited to about 0.5 MW/m^2.

4.1.6. Embrittlement

In unirradiated conditions, type 316LN is very ductile and maintains its high ductility and toughness even after prolonged aging. Its welded joints seldom need post-weld annealing. When irradiated at low temperatures, particularly in the temperature range of 200–320 °C, its ductility and toughness decrease with increasing irradiation dose. Its tension stress–strain curve may show little or no hardening capacity. At higher irradiation temperatures, irradiation hardening is negligible, but the steel becomes prone to irradiation swelling at doses greater than about 20 dpa, the level of which varies with temperature and material state.

4.1.7. Future perspectives

Stainless steel will probably remain one of the most widely used materials in the future fusion power reactors. It does not have a lower temperature limit in unirradiated conditions and its upper temperature window can be as high as 700 °C. Its low temperature embrittlement (at $T <\approx 300$ °C) is somewhat offset by its good service experience in light water reactors (at 280–320 °C) and by the fact that its toughness is better than at 200–300 °C when cooled down to room temperature. The effects of high He/dpa and 14 MeV neutron irradiation are, however, of concern and remain to be fully analyzed.

The three main drawbacks of 316LN for application in blanket structure of FPR are low surface heat capability, low irradiation swelling resistance at high doses when used at temperatures higher than about 350 °C and high nuclear activation.

Using the steel in cold-worked state can allow a slight increase in surface heat capability and can at the same time improve the irradiation swelling resistance. But such measures reduce the ductility and their beneficial effects may be lost during high temperature exposures. Utilization of other grades of 316 (e.g. 316Ti) or other types of SS, could also be envisaged for improving the swelling resistance. But most of these steels have been developed for nuclear fuel subassemblies (cladding and wrappers) and lack thick section structural material's data base.

4.2. Ferritic/martensitic steels

4.2.1. General description

Several conventional grades of this steel are already code qualified (e.g. T91, modified 9Cr–1Mo) [13]. One of the reduced activation grades currently investigated, F82H steel (Fe–8Cr–2W–Ta–V), has a good data base [14,15]. Data extracted from the Appendix A/DISDC of this steel is used here [14]. Eurofer (Fe–9Cr–1W–Ta–V), the reduced activation steel preferred in Europe, is in its early stages of characterization. For an overview of ferritic/martensitic steels and recent results see Ref. [16] and its sub-references.

4.2.2. Tensile properties

As shown in Fig. 3, the strength of F82H steel continuously decreases with increasing test temperature and the drop becomes sharper at above about 550 °C. As a result, F/M steels are seldom used at above 600 °C. The difference between the YS (R_p or S_y) and the UTS (R_m or S_u) of F82H is small and $1/3$ S_{umin} determines S_m.

4.2.3. Creep properties

Fig. 4 shows the evolution of the initial applied stress versus time to rupture at several temperatures. At temperatures higher than 600 °C creep strength is sharply reduced. The average stress-to-rupture in 10 000 h becomes less than 100 MPa.

Table 3
Physical properties [12] and surface heat capability factor

Temperature (°C)	E (GPa)	α_i (10^{-6} K^{-1})	k (W/K m)	C_p (J/kg K)	M (kW/K m)
300	170	18.5	17.95	529	1.22
400	161	19.3	19.39	550	1.22
500	153	20	20.82	571	1.25
600	145	20.8	22.25	592	1.33
700	137	21.4	23.69	613	1.38

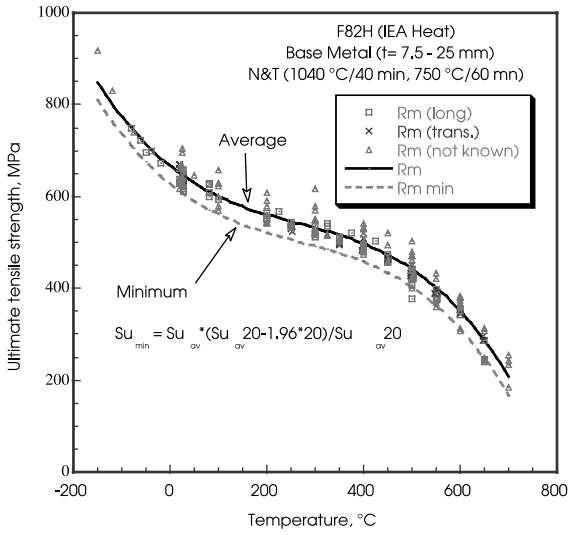

Fig. 3. Minimum and average ultimate tensile strength of F82H base metal [14].

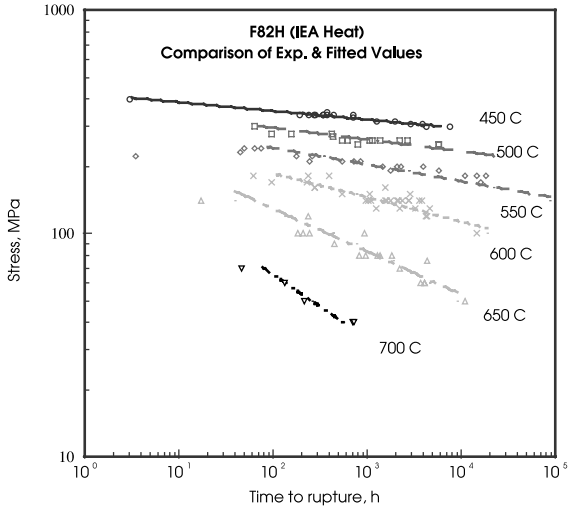

Fig. 4. Comparison of experimental creep-rupture results of F82H steel with trends derived from master creep curve [14].

4.2.4. Fatigue properties

Fatigue properties of F82H are still sparse and design curves deducted are tentative. However, since the properties of these steels are similar to those of the conventional modified 9Cr–1Mo steels [13], one can use the latter as an interim measure.

One of the difficulties in designing with F/M steels and indeed other high strength alloys discussed in this paper is the treatment of initial stress during creep–fatigue interaction. Significant cyclic softening and stress relaxation could occur in these materials. If the reduction in stress is not taken into account, then the thermal creep damage will be over estimated. For instance, the initial stress corresponding to a total strain amplitude of 0.3% (slightly more than the yield stress), corresponds to a stress level of about 350 MPa, and hence an average rupture time of less than 1 h at 550 °C.

4.2.5. Surface heat capability

Surface heat capability of F82H is better than stainless steels by a factor of 2–3 (Table 4). F82H has a higher S_m, a lower coefficient of thermal expansion and a higher coefficient of conductivity. Nevertheless, at temperatures above 550 °C, the strength of F82H is reduced and its superiority over 316LN is diminished.

4.2.6. Embrittlement

F82H steel has a bcc structure and like other materials of this type exhibits a transition from ductile to brittle fracture at low temperatures. However, in the unirradiated conditions its DBTT is around −50 °C and well below room temperature. Increases observed in the DBTT after aging or welding (with PWHT) also remain moderate. It is only after irradiation at temperatures less than about 300 °C, where hardening is important (Fig. 5), that the increase in DBTT becomes of concern. At higher irradiation temperatures the DBTT hardly changes and the material is expected to exhibit good resistance to swelling at doses up to 100 dpa if not higher. The effect of high He-to-dpa ratio on DBTT is not yet correctly reproduced in these alloys and needs to be investigated.

4.2.7. Future perspectives

RAFM steels share many advantages of stainless steels (cost, availability, service experience), have a better surface heat capability and a lower activation.

Table 4
Physical properties [14] and surface heat capability of F82H steel

Temperature (°C)	E (GPa)	α_i (10^{-6} K^{-1})	k (W/K m)	C_p (J/kg K)	M (kW/K m)
300	203	11.1	33.4	544	4.32
400	197	11.7	33.0	586	3.92
500	189	12.0	32.7	644	3.48
600	178	12.3	32.3	728	2.74

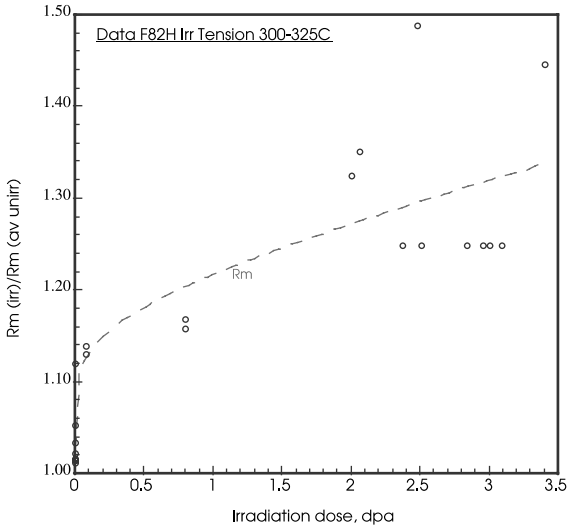

Fig. 5. Effect of irradiation on ultimate tensile strength (R_m) of F82H base metal [14].

F/M steels have four main drawbacks for application in FPR:

- In order to obtain a fully martensitic microstructure, the steel has to be quenched from the normalizing temperature. It is not certain that adequate cooling rates can be maintained in thick sections or during manufacturing techniques such as HIPing, often required for fabrication of complex blanket components.
- Their irradiation embrittlement at temperatures <250–300 °C may be further aggravated by higher amounts of He and H generated under fusion spectrum.
- They have a relatively low upper temperature window (less than 600 °C), that is even lower on the liquid metal side (limited to 480–500 °C due to excessive corrosion rate). The latter problem can be alleviated, e.g., through surface coating with Al_2O_3 [2].
- Their welded joints have to be post-weld heat treated.

The strength of RAFM steels can be improved through utilization of oxide dispersion strengthened (ODS) grades. The ODS steels contain small particles of Y_2O_3 and/or TiO_2 dispersed in a ferrite matrix. They are currently being developed for fission and fusion applications in Japan [17], Europe [18,19], and the United States [20]. Most of the work done in US and Japan are on higher chromium content steels, while in Europe, ODS alloys with Eurofer steel composition are also developed [18].

Significant increase in tensile and creep strengths can be obtained with ODS, but at the expense of toughness and weldability. Ukai et al. [17] have reported important gains with 0.3% Ti and 0.25% yttria (Fe–11.7Cr–1.92W), while maintaining good fabricability (Table 5).

Table 5
Comparison of tensile and creep-rupture strengths of F82H steel and an ODS steel at 700 °C [17]

Alloy	UTS (MPa)	1000 h creep rupture (MPa)
F82H	200	32
ODS (11.7Cr)	370	150

Nevertheless, it is unlikely that the ODS steels would satisfy structural integrity criteria for critical components in the near future. Their most promising near term application is probably in association with conventional steels. One of the ideas to explore is HIPing of a small layer of ODS composition upon the conventional steel composition or making gradient composition panels. The reason for this is that high temperature zones are localized at the surface and do not extend more than 1 or 2 mm through the metal. As a result, a gradient material with ODS composition at the surface would combine high temperature resistance required at the surface, with good toughness through the bulk.

4.3. Vanadium alloys

4.3.1. General description

Vanadium alloys occupy a special place amongst the refractory metal alloys and are treated apart here. They have been extensively investigated over the past few years for fusion [21–29], with V–4Cr–4Ti emerging as favored alloy composition [21].

4.3.2. Tensile properties

The strength of V–4Cr–4Ti is relatively constant in the range of 200–800 °C [22–25]. The minimum tensile strength is about 320 MPa corresponding to a tentative S_m value of about 130 MPa. The yield strength is also almost constant in the temperature range of 200–800 °C, and varies within a scatter band of 200–250 MPa. The uniform (7–20%) and total (20–30%) elongations as well as the reduction of area (80%) in this temperature range are high. However, stress–strain curves obtained at 1.1×10^{-3} s^{-1}, show serrations, most likely due to dislocations interaction with dissolved O, C, N interstitial solutes [23].

4.3.3. Creep properties

Vanadium alloys have a better creep resistance than F/M and stainless steels. Their creep resistance can be further improved by increasing Cr and Ti contents [21]. However, most of the actual data are obtained at temperatures up to 600 °C and are for relatively short du-

rations (<4000 h at 600 °C). At higher temperatures and longer exposure times, oxygen pickup from surrounding atmosphere may adversely affect the properties.

4.3.4. Fatigue properties

Only limited data have been generated for the vanadium alloys [27,28]. At room temperature fatigue data for V–5Cr–5Ti and V–15Cr–5Ti tested in high vacuum (1.3×10^{-11} bar) are slightly better than the conventional 316 SS tested in air at low cycles ($<10^4$), but become much better at higher cycles. However, fatigue resistance of vanadium alloys can be severely degraded with oxygen contamination at high temperatures [26].

4.3.5. Surface heat capability

Vanadium alloys have an excellent surface heat capability due to their low coefficient of linear thermal expansion and high thermal conductivity (Table 6). Values of $M > 4$ are calculated for an $S_m = 105$ MPa.

4.3.6. Embrittlement

Most of the irradiation experiments on vanadium alloys are performed at test temperatures above 400 °C [22,24,25,29–33]. At such temperatures hardening is negligible and V–4Cr–4Ti maintains its good ductility. At lower temperatures, the hardening is very important and uniform elongation becomes practically nil (Fig. 6).

4.3.7. Future perspectives

Vanadium alloys will remain very attractive for FPR due to their low activation and high surface heat flux capability. They also have a good compatibility with lithium at least up to 600 °C. At higher temperatures interstitial solute pickup and corrosion rates may become significant. The most likely application of vanadium alloys would be with low-pressure Li coolant. The feasibility of use with He coolant or Flibe is much lower. Their operating temperature window can be tentatively put in the range of 400–700 °C, provided fully adherent self healing insulator coatings can be successfully developed. The lower temperature bound is governed by irradiation embrittlement. The upper temperature is bound by thermal creep, helium embrittlement or chemical compatibility/corrosion depending on the solution

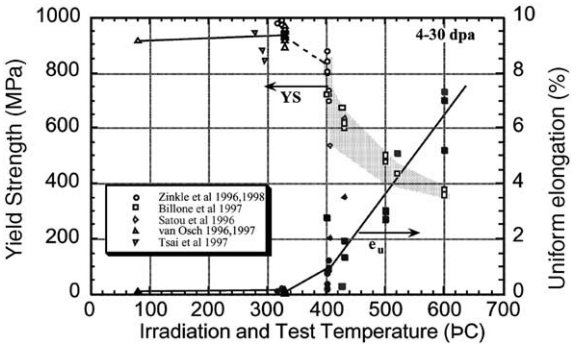

Fig. 6. Yield strength and uniform elongation of irradiated V–(4–5)% Cr–(4–5)% Ti alloys [29].

employed. However, the results reported at various European fusion program meetings show that several major obstacles still limit large-scale utilization of vanadium alloys.

4.4. Ceramic composites

4.4.1. General description

In this category SiC_f/SiC has established itself as the reference material. However, there is not one commercial SiC_f/SiC, but many SiC_f/SiC and they are constantly evolving [9,10,34–46]. Any conclusions drawn here can be outdated in the near future.

Table 7 shows several commercial SiC-based fibers and bulk SiC with some of their properties [10,36–39]. In Europe, most of the recent work has been on Cerasep N4-1 supplied by Snecma (using Hi-Nicalon), which follows the Cerasep N3-1. A good review of the work done is given in [10].

The chemical composition, density, elastic constants, thermal conductivity, and neutron radiation resistance of cg-Nicalon and non-stoichiometric Hi-Nicalon fibers are considerably different from those of bulk crystalline SiC which constitutes the matrix [36]. Recent fibers such as Hi-Nicalon Type S [36] and Dow Sylramic [37] are expected to produce improved composite properties in the unirradiated and irradiated condition compared to former fibers.

Table 6
Physical properties [21] and surface heat capability of V–4Cr–4Ti

Temperature (°C)	E (GPa)	α_i (10^{-6} K^{-1})	k (W/K m)	C_p (J/kg K)	M (kW/K m)
300	125	10	30.4	505	4.60
400	124	10.3	31.3	522	4.61
500	123	10.7	32.1	533	4.62
600	122	11	33.0	540	4.63
700	121	11.4	33.8	545	4.63

Table 7
Comparison of properties of commercial SiC-based fibers and bulk SiC [10,35]

	cg-Nicalon	Hi-Nicalon	Hi-Nicalon type S	Dow Sylramic	Cerasep N3-1	Bulk SiC
Diameter (μm)	14	12–14	12	10		–
Tensile strength (GPa)	2.0–3.0	2.8–3.4	2.6–2.7	2.8–3.4	3.00	~0.1
Elastic modulus (GPa)	170–220	270	420	390–400	200	460
Density (g/cm^3)	2.55	2.74	2.98–3.10	3.0–3.10	>2.4	3.25
Coeffecient of linear thermal expansion (10^{-6} K^{-1})	3.2	3.5	–	5.4	4 (1000 °C)	4.0
Thermal conductivity at 20 °C (W/K m)	1.5	4	18	40–45	15	100–350
Oxygen content (wt%)	11.7	0.5	0.2	0.8	–	0.0
C/Si atomic ratio	1.31	1.39	1.05	1.0	–	1.0

4.4.2. Tensile properties

Most of the available data on ceramic matrix composites have been generated using flexural bend strength tests (3- or 4-point bending) and not uniaxial tensile testing with generation of engineering data. In addition, the notion of failure in ceramic matrix composites is different from that in metallic materials. In metallic materials formation of cracks are synonyms of failure while composites are engineered to produce a moderate amount of fiber pullout during deformation. The optimum tensile toughness generally occurs in ceramic composites with tensile elongations in the order of 0.2–0.5% (in the order of 0.2% offset proof stress in metals).

The ultimate tensile strengths of several different grades of SiC_f/SiC composites containing 40 vol.% fibers (0/90° weave) have been recently measured by tensile testing [40,41]. The UTS obtained ranges from 200 to 280 MPa at room temperature. Little reduction in strength is observed up to 1000 °C. Tensile data for more recent ceramics are not expected to be very different. In fact, the new composites supplied by Snecma, N4-1, have lower strength (bend strength) than the previous N3-1: (553 ± 101) MPa and (674 ± 85) MPa, respectively, at 20 °C [10]. Dynamic flexural modulus values of N4-1 are higher (300–280 GPa from RT to 1100 °C) than N3-1 by about 50–80 GPa.

Deducting an S_m value from such information is hazardous. If the reported values for proportional stress limits are used, then very low S_m values are obtained (on the order of 40 MPa). Even if the UTS values are considered, values less than or equal to 130 MPa are obtained.

4.4.3. Creep properties

There are little information available on the thermal and irradiation creep of SiC_f/SiC. Zinkle and Snead [35] has made a rough estimate of irradiation creep using data obtained for monolithic SiC and suggests that the irradiation creep constant may be $K \cong 10^{-12}$ (Pa dpa)$^{-1}$ at 500–1100 °C [42], which is lower than the value observed for some other ceramics [43].

4.4.4. Fatigue properties

Little information is available on fatigue properties of SiC_f/SiC composites [46].

4.4.5. Surface heat capability

The elastic constants for SiC_f/SiC composites depend on the details of the fabrication procedure. Values ranging from 140 to 460 GPa have been reported (here we assume a value of 270 GPa). Poisson's ratio for bulk SiC is taken equal to 0.18 between 20 and 1000 °C [35].

The thermo-physical properties of SiC_f/SiC composites (particularly thermal conductivity) are also dependent on the fabrication procedure. The measured linear coefficient of thermal expansion (α_i) for SiC_f/SiC composites fabricated with cg-Nicalon fibers (40 vol.% fibers) are $(2.5–3) \times 10^{-6}$ K^{-1}, with no pronounced dependence on temperature between 20 and 1000 °C [45].

The thermal conductivity of SiC_f/SiC composites is strongly dependent on the processing conditions, type of fiber, and fiber architecture [46]. The upper limit for linear thermal conductivity corresponds to that obtained in single-crystal and high-purity CVD SiC, with maximum values of ≅320 W/K m at room temperature and 78 W/K m at 1000 °C (Fig. 7). Unlike the case for metals (where the thermal conductivity is dominated by electron transport), irradiation can cause a significant reduction in the thermal conductivity of SiC_f/SiC composites. The degradation is particularly large at low irradiation temperatures. The thermal conductivity of a SiC/SiC_W composite irradiated to 43 dpa at 1000 °C ranged from ≅12.5 W/K m at 400 °C to ≅10 W/K m at 1000 °C [47].

Table 8 presents an estimate of the surface heat capability of SiC_f/SiC composites using information extracted from [47]. If the thermal conductivity values in

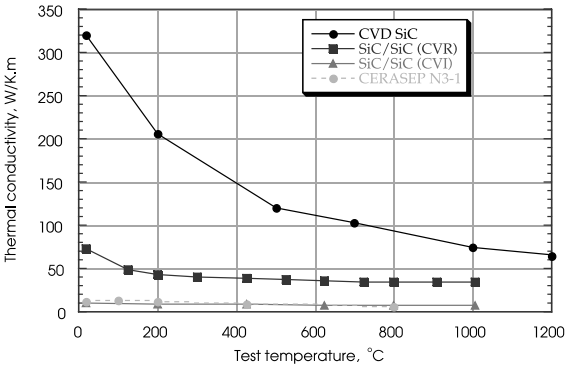

Fig. 7. Comparison of the transverse thermal conductivity of monolithic CVD SiC and three grades of SiC_f/SiC composites [10,35].

the unirradiated conditions are used, then significantly higher M values are obtained.

4.4.6. Embrittlement

Toughness is the weak point of ceramics and ceramic composites, particularly when they are irradiated. First PIE results [34] show a substantial reduction in the fracture toughness of composites even at a very low fluence (1.6×10^{19} n/cm^2).

Unlike metallic materials, where some of the irradiation damage can be recovered through heat treatment, the damage in ceramics is often permanent (debonding) and those due to defect clusters cannot be recovered at normal operating temperatures. For instance, neutron irradiation can produce a significant decrease in the flexural strength of SiC_f/SiC composites fabricated with cg-Nicalon fibers, due to neutron-induced densification of the fibers which causes debonding at the matrix/fiber interfaces [48,49]. Strength decreases up to a factor of two have been observed in some cases. Improved irradiated behavior is predicted for composites containing new SiC fibers such as Hi-Nicalon, MER-999, and Dow Corning Sylramic fibers [38,50–52].

A summary of the radiation-induced swelling in monolithic SiC as a function of irradiation temperature have been made by Zinkle and Snead [35] using data reported in [50,52–56]. Three distinct temperature regimes have been identified. At low temperatures (<150 °C), a crystalline-to-amorphous phase transition is induced at relatively low doses (0.1–1 dpa). The amorphous phase has a much lower density compared to the crystalline phase, which results in ≅11% swelling [56]. Bulk SiC exhibits moderate swelling due to neutron irradiation at temperatures between 150 and 900 °C. The minimum temperature for significant void swelling in SiC is somewhat uncertain. Early work by Price [55] indicated that significant void swelling did not occur for irradiation temperatures below ≅1100 °C. However, two recent studies have observed high volumetric swelling in SiC irradiated at ≅1000 °C [50,52]. Detailed analysis of the above results suggests that some specimens may have been contaminated or influenced by presence of boron [46]. Further work is needed to determine the minimum temperature for void swelling in SiC. The effects of fusion-relevant helium generation on the dimensional stability of SiC has not been adequately studied. Very high values of He and H generations have been reported in SiC_f/SiC [1]. SiC_f/SiC ceramic composites are still at their very early stages of development.

4.4.7. Future perspectives

Joining of ceramic composites is another difficulty to surmount. Recent work on optimization of brazing has allowed control of the infiltration of the braze in the porous composite and adaptation of the thermo-mechanical behavior of the braze against the SiC_f/SiC composite. Nevertheless, the majority of failures still occur in the joint. The N3-1 joint shear strength ranges between 54 and 200 MPa at 20 °C and 89–97 MPa at 800 °C. The shear strength obtained using N4-1 is lower (14–62 MPa at RT and 18–76 MPa at 800 °C). Joints prepared using polymers and powders show even lower performance (1–10 MPa) [34].

Chemical compatibility of SiC_f/SiC with Pb–17Li has been measured for short duration static exposures. No reaction is observed between Pb–17Li and N3-1 after exposure at 800 °C for 3000 h [34]. Penetration of the Pb–17Li is limited to the open porosities. Compatibility between N3-1, N4-1, PIP-3D composites with and without CVD coating and Pb–17Li will be tested at

Table 8
Tentative use of physical properties for calculating the surface heat capability of SiC_f/SiC composites

Temperature (°C)	E (GPa)	α_i (10^{-6} K^{-1})	k (W/K m)	C_p (J/kg K)	M (kW/K m)
20	400	2.5	10.0	1287	0.84
300	400	2.5	10.0	1187	0.84
500	400	2.5	10.0	1152	0.84
700	400	2.5	12.5	1133	1.05
1000	400	2.5	12.5	1120	1.05

S_m assumed = 70 MPa (1/3 of 210 MPa composite strength).

550 °C for 6000 h under flowing conditions (1 m/s) in the LiFus2 facility (ENEA) [34].

The permeation barrier is yet another obstacle to surmount. ENEA has explored utilization of low activation glass ceramic coatings in order to allow He pressures up to 8 MPa. Permeability reduction factors of up to 100 times have been obtained.

The minimum operating temperature limit of SiC_f/SiC composites will be determined by either the crystalline to amorphous transition temperature (≅120 °C for fusion reactor damage rates) [56], or else radiation-induced degradation in the thermal conductivity (400 °C). The maximum temperature limit will likely be determined by void swelling considerations (1000 °C), although there are not sufficient data at elevated temperatures (900–1400 °C) to make a clear determination.

4.5. Refractory metal alloys

4.5.1. General description

Refractory metal alloys are divided into groups V (V, Nb and Ta) and VI (Cr, Mo, and W). Group V alloys are easier to fabricate than group VI alloys but both groups have bcc structures and are prone to low temperature brittle fracture. Vanadium alloys were discussed separately above, others are briefly discussed below.

4.5.2. Chromium and chromium alloys

They are currently investigated in Europe for fusion application. The European activity in 2000, part of which has been reported in [34], has been mainly dedicated to characterization of a pure Cr and a Cr alloy supplied by Plansee (Ducropur = 99.96% pure Cr and Ducrolloy = $Cr_5Fe_1Y_2O_3$). The work done also includes the effects of thermo-mechanical treatments in order to improve the ductility. The Cr alloy was prepared using mechanical alloying, followed by pressing, sintering and HIPing.

Both alloys show a brittle behavior in the as-HIPed conditions in bending and tension tests at room temperature. Plastic deformations are reported between 200 and 250 °C and above 400 °C. The linear elastic fracture toughness (K_Q) of pure chromium in the unirradiated state increases from 12 MPa $\sqrt{m}$ at 290 °C to a value of 500 MPa $\sqrt{m}$ at 320 °C, even then the final fracture occurs in a cleavage mode. Ducrolloy exhibits low toughness values at temperatures up to 600 °C (3.9–10.9 MPa $\sqrt{m}$). Even at 740 °C its toughness is about 22.4 MPa $\sqrt{m}$. The DBTT of both the Cr and Cr alloy are expected to shift to higher temperatures after irradiation.

In bending tests, the DBTT of Cr is only slightly lower (220–270 °C), but that of the Cr alloy is considerably lower (400 °C). In tension tests, the Cr alloy shows a higher strength but also a higher brittleness and sensitivity to surface defects (Table 9). Mechanical strengths of both alloys decrease rapidly at temperatures above 600–800 °C.

An improvement in ductility and a significant increase in fracture strength are reported in [34] by predeformation in tension and in bending, through equal channel angular extrusion and die compression.

The main advantage of Cr alloys, in general, resides in their excellent corrosion and oxidation resistance. Coupled with their high hardness and compressive yield strength (for Ducrolloy 1222–1000 MPa at 20–200 °C), they are primarily used as special purpose materials (e.g. coating, plating). Their relatively high lower-temperature limit (300–800 °C), and relatively low upper-temperature limit (about 800 °C from tension tests) limit their temperature window. Also, the protective oxide layer (Cr_2O_3) becomes unstable at higher temperatures

Table 9
Tensile strength in MPa and strains in % of DP and DL (Yield stress $\sigma_{0.2}$ or σ_{UYP}) reported in European meetings [34]

Temperature (°C)	Cr				$CrFeY_2O_3$			
	$\sigma_{0.2}$	σ_{UTS}	ε_a	ε_l	$\sigma_{0.2}$	σ_{UTS}	ε_a	ε_l
25	329	329		0.6	565	565		
25	199	196		0.6	570	570		
200	199	196	2.9	3.1	549	549		
200					584	584		
400	106	245	85	51	783	783		
400	110	254	85	47	752	752		
600	97	224	88	35	492	545	11	11
600	129	214						
800	85	138	95	38	180	191	8.5	9.1
800	80	165			168	170	38	21
960	63	85	85	30				
980					125	126	8.5	8.6

in vacuum and transforms to CrO_3 with a possible loss of Cr [11]. Nevertheless, the low coefficient of linear thermal expansion (at RT about 6.5×10^{-6} K^{-1}), high conductivity (32 W/K m) and high modulus (248 GPa) of chromium give a better thermal heat capability than that of steels.

4.5.3. Niobium alloys

The alloys C-129Y (Nb–10W–10Hf–0.2Y), Cb752 (Nb–10W–2.5Zr), FS-85 (Nb–10W–28Ta–1Zr) and WC3015 (Nb–14.3W–28.5Hf–1.2Zr–4.7Ti–0.66Ta) are not low activation materials. They have been mainly investigated for one of the versions of the thermal protection system of the space shuttle [11,57–59]. Amongst the niobium alloys mentioned above, FS-85 has superior weldability, fabricability and creep resistance [11]. Nb–1%Zr is a better known alloy and has had some applications in the nuclear industry.

The maximum service temperature of niobium alloys can be as high as 1370 °C, although their tensile strength drops from 450 MPa at about 600 °C to 100 MPa or less at above 1200 °C (Fig. 8). Their upper service temperature most likely would be limited by thermal creep to about 1200 °C. With a low coefficient of linear thermal expansion ($8–10 \times 10^{-6}$ K^{-1}) and a high thermal conductivity (50–74 W/K m), niobium alloys offer an excellent surface heat flux capability (higher than 10).

Niobium alloys have shown good compatibility with static and flowing lithium at least at temperatures up to 1000 °C [2]. Nevertheless, future perspectives for niobium alloys use in FPRs are limited. There are serious safety and waste disposal considerations with their utilization at all temperatures. Also there is a risk of severe oxidation at high temperatures if exposed to air.

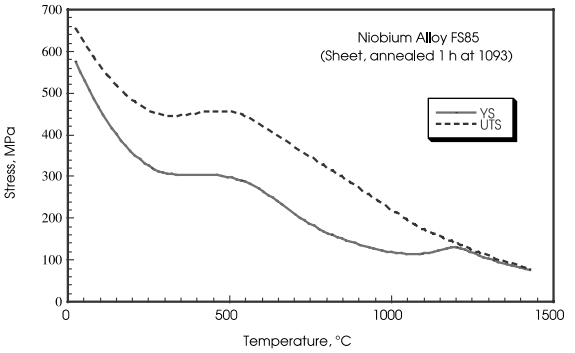

Fig. 8. Tensile properties versus temperature for FS85 sheet annealed 1 h at 1093 °C. Total elongation is greater than 10% [11].

4.5.4. Molybdenum and its alloys

These alloys such as TZM, are also high activation materials. In addition, they have poor ductility. Addition of Re to Mo not only increases strength, through solution hardening, but also improves ductility [61,62]. As a result, Mo–Re alloys had received particular attention during the French space reactor program [61]. Materials tested in that program included Mo, Mo–13%Re, Mo–41%Re. The test program covered bend, tension and creep. Re containing alloys show good ductility in the unirradiated condition even at −120 °C (Table 10). They also show good creep resistance at 1200 °C in the annealed condition. However, recrystallization may occur during longer creep exposures at such high temperatures that would accelerate creep (Fig. 9).

Results obtained from microstructural and mechanical tests performed on irradiated specimens have shown that at such high temperatures the risk of significant cavitations or irradiation hardening is negligible. They

Table 10
Tensile properties of Mo–Re alloys, all tests are performed on cylindrical specimens (2 mm in diameter and 10 mm in gauge length) at a strain rate of 10^{-4} s^{-1} [61]

Temperature (°C)	Alloy	YS (MPa)	UTS (MPa)	UE (%)	TE (%)
−196	Mo–13Re	1348[a]	1407	<0.02	<0.02
	Mo–41Re	1255	1545	7	7
−120	Mo–13Re	985	985	3.5	3.5
	Mo–41Re	1029	1137	7	8
−50	Mo–13Re	545	652	6	6
	Mo–41Re	971	1029	5	5
20	Mo	590	625	13	40
	Mo–13Re	528	603	6	7
	Mo–41Re	813	913	6	7
1100	Mo–13Re	210	213	0.6	24
	Mo–41Re	289	307	1.5	34

[a] Yield stress at 0% offset.

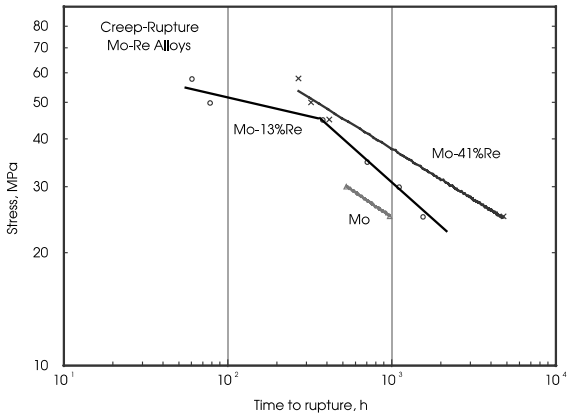

Fig. 9. Stress versus time to rupture at 1200 °C for Mo and Mo–Re alloys [61].

have, nevertheless, revealed that accelerated microstructural transformations in the three materials would occur with the formation of Re rich phases, particularly in the higher Re alloys. Re containing alloys also have a poor fusion weldability due to segregation of Re.

Pronounced radiation hardening have been reported for Mo and Mo alloys such as TZM and Mo–Re up to about 700 °C [62–66]. For instance, significant hardening and very low ductility values are noted after irradiation at 700–800 °C and damage levels of 5–20 dpa. The upper temperature window of Mo and Mo alloys will be most likely determined by thermal creep at 1000–1200 °C, thus giving a temperature window of 800–1200 °C.

Future perspectives for molybdenum alloys in FPR is narrow. Poor ductility and high activation of these alloys will most likely limit their application in less critical or unirradiated zones.

4.5.5. Tantalum alloys

The alloy Ta–8% W–2% Hf (T-111)has been largely investigated in the US space program [67,68]. Zinkle [69] has recently summarized its thermo-physical and mechanical properties for the US APEX project.

Results obtained from tensile tests performed on stress-relieved and recrystallized specimens have been reported in [69–73]. The latter is more relevant to long service durations at higher temperatures but in any case the properties of the alloy in the two states merge at 1200 °C and above.

There have been numerous studies of the creep and stress-rupture behavior of unirradiated T-111 at temperatures up to 1600 °C (0.57 T_M) [74–76]. The stress to produce 1% strain in T-111 in 1000 h is ≅110 MPa at 1100 °C and ≅50 MPa at 1250 °C [75]. Using a 1000 h creep-rupture stress level of 100 MPa as a guideline, the maximum operating temperature of T-111 is 1150–1200 °C [75]. Using the more conservative creep criterion of 1% plastic strain, the maximum operating temperature of T-111 for an applied stress of 100 MPa is 1000 °C for long-term (7 year) operation [74].

Surface heat flux capability of T-111 is excellent (>11 kW/K m). Young's modulus has been measured from −100 to 2000 °C (180–160 GPa between 20 and 1000 °C) [71,72]. The mean coefficient of linear thermal expansion (α_m) is very similar to that of pure Ta and Ta–10W, and varies from 5.9×10^{-6} K^{-1} at room temperature to 7.6×10^{-6} K^{-1} at 1650 °C [71,72,75]. The thermal conductivity varies from ≅42 W/K m at room temperature to ≅56 W/K m at 1350 °C.

The DBTT of unirradiated T-111 has generally been estimated from reduction in area measurements on unnotched tensile specimens [72,77]. The resultant DBTT value (≅−200 °C) is obviously a severe underestimate of the value that would be obtained with conventional impact specimens. There are no known DBTT studies on irradiated T-111, although a significant increase in the DBTT would be expected for irradiation at temperatures up to at least 650 °C, based on the large increase in hardening associated with these relatively low irradiation temperatures (<0.3 T_M). The lower temperature limit of Ta-111 is hence assumed equal to 650 °C.

Future Perspectives: Tantalum alloys are easier to fabricate than Cr, Mo and W alloys and have excellent high temperature thermal creep properties [76–81]. Several forced-flow corrosion and engineering loop studies have demonstrated that T-111 has good compatibility with liquid lithium at least up to temperatures of ≅1370 °C [76–79]. Ta alloys have also exhibited good compatibility with other liquid metals, including Na, K and Pb to ≅1200 °C [76–79].

Their main drawbacks is embrittlement at temperatures less than about 700 °C, that gives them a tentative temperature window of 700–1200 °C. Moreover, Smith et al. [1] report very high dose rates for Ta, 10^6 Sv/h for 1 month after 3 years of operation at 5 MW/m^2, as compared with 1000 for ferritic steels.

4.5.6. Tungsten and tungsten alloys

These alloys suffer from similar drawbacks as the other refractory metal alloys. Their fabrication costs for producing finished products is high and lack satisfactory full penetration weldability to this date. They have in contrast a very high temperature window (1600 °C) and do not suffer from high activation.

Probably the most limiting factor for utilization of tungsten alloys as structural material is their low toughness. As shown in Fig. 10 [82–88], the fracture toughness of pure tungsten is less than 100 MPa$\sqrt{m}$ at all temperatures, with a typical value at 1000 °C of ≈30 MPa$\sqrt{m}$. This is similar to the lower shelf toughness of irradiated ferritic–martensitic steels and vanadium alloys.

Some improvements may be obtained through alloying with dispersed oxide particles (e.g. ThO_2), Re

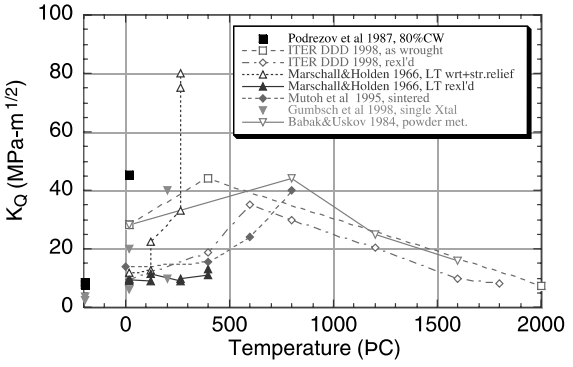

Fig. 10. Temperature-dependent fracture toughness K_Q of pure tungsten in various thermo-mechanical conditions [60].

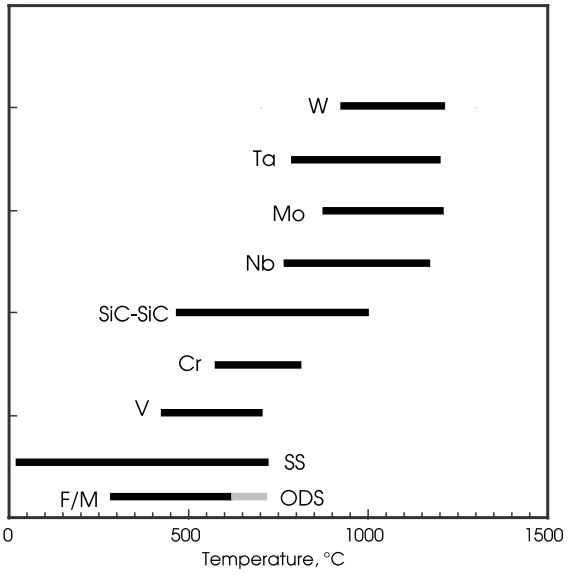

Fig. 11. Tentative temperature window of the materials discussed.

and Ni [84,85]. However, tensile elongations of ≈0 have been reported for W irradiated at 400 and 500 °C to fluences of <2 dpa (in W) [64,88,89]. Severe embrittlement (DBTT > 900 °C that can also be assumed as its lower temperature window) has also been reported for un-notched bend bars of W and W–10% Re irradiated at 300 °C to about 1 dpa [90].

Future perspectives for tungsten alloys will most likely reside in functional materials, where their high-temperature capability can be put in service at very high temperatures (>1400 °C). Despite their corrosion/chemical compatibility with Li and Pb–Li, good thermal heat capability (4–8 kW/K m), due to low coefficient of linear thermal expansion (3.9×10^{-6} K^{-1}), high conductivity (about 85 W/K m) and Young's modulus (352–397 GPa), their very low toughness bars them from use in critical structural components.

5. Discussion

The above assessment shows that austenitic and ferritic/martensitic steels will remain the foremost contenders for the future FPR blanket system despite uncertainties in the areas of irradiation induced embrittlement at low temperatures and high He/dpa ratio effects. This is due to the fact that neither one of the advanced high temperature materials examined so far, has the maturity or the reliability needed for application in critical components. Nevertheless, the same assessment also shows that both stainless and F/M steels lack high temperature surface heat capability needed for an efficient fusion power system.

Some improvements in the properties of the advanced high-temperature materials are expected by the time an FPR is put in service, but it is unlikely that the inherent problems associated with these materials would disappear. SiC_f/SiC composites should continue to suffer from fiber/matrix, thermal conductivity, joining and low toughness related issues. Refractory metal alloys would also continue to suffer from severe irradiation embrittlement up to relatively high temperatures (400–900 °C depending on the alloy).

The problem of utilization of refractory metal alloys or ceramic composites as structural materials has, therefore, to be mitigated not separately by materials R&D alone, but in conjunction with the blanket and system design. Classification of materials and components according to their safety and structural integrity implications, when the FPR design is adequately advanced, will help in this respect. Fig. 11 shows tentative temperature windows for the materials discussed in this paper.

6. Conclusions

- Stainless steels and ferritic/martensitic steels will remain the main contenders for the future FPR blanket system despite uncertainties in the areas of irradiation induced embrittlement at low temperature and high He/dpa ratio effects.
- F/M steels have a lower temperature window of 250–300 °C and an upper temperature limit of 550–600 °C. With selective utilization of ODS steels, the upper temperature window of F/M steels can be increased to 650 °C. Also with an appropriate coating the problem of excessive corrosion in liquid metals at $T > 480$ °C can be resolved.

- Vanadium alloys, with a temperature window of 400–700 °C, remain very attractive for FPR due to their high surface heat flux capability, but still lack industrial maturity and their performance is tied to development of a reliable fully adherent self healing insulator coating.
- New fibers developed for SiC_f/SiC composites are expected to improve the compatibility with the matrix and hence the properties. With their high temperature window (400–1000 °C), SiC_f/SiC composites offer increased efficiency. Their utilization as structural material in critical components still has to surmount many obstacles.
- Refractory metal alloys (Cr, Mo, Nb, Ta and W) are most suited for special purposes or functional applications. Molybdenum and niobium pose safety and waste disposal problems, while tantalum suffers from high decay heat, and chromium and tungsten from low toughness.

References

[1] D.L. Smith, S. Majumdar, M. Billone, R. Mattas, J. Nucl. Mater. 283–287 (2000) 716.
[2] S.J. Zinkle, N.M. Ghoniem, Fusion Eng. Des. 51&52 (2000) 55.
[3] Report on the European materials assessment meeting, Karlsruhe, 5–8 June 2001, edited by EFDA Close Support Unit, Garching, Germany.
[4] J. Davis (Ed.), ITER Materials Properties Handbook, ITER Document no. S74 MA 2, 97-12-12 R 0.2, 4th Ed., 1997.
[5] Proceedings of ITER Materials Assessment meeting, 1-5/12/97, ITER, Garching, Germany.
[6] M. Seki, R. Matera, F. Tavassoli, J. Davis, D. Smith, J. Nucl. Mater. 271&272 (1999) 569.
[7] Report of the IEA workshop, working group meeting on ferritic/martensitic steels for Fusion Applications, JAERI, Tokyo, Japan, 2–3 November 2000.
[8] Report of the Fifth IEA Workshop on Vanadium Alloys for Fusion Applications, October 30–November 1, 2000, Tokyo University, Tokyo.
[9] Report of the Fourth IEA working group meeting on SiC_f/SiC for fusion application, Frascati, Italy, October 12–14, 2000.
[10] G. Aiello, L. Giancarli, H. Golfier, J.-F. Maire, Modeling of mechanical behaviour and design criteria for SiC_f/SiC composite structures in fusion reactors, Fus. Eng. Design., to be published.
[11] A.-A.F. Tavassoli, Aeronaut. J. 3 (1972) 152.
[12] A.-A.F. Tavassoli, F. Touboul, J. Nucl. Mater. 233–237 (1996) 51.
[13] J. Waering, A.-A.F. Tavassoli, in: S.V. Möller, J.D. Riera (Eds.), Transactions of the 13th International Conference On Structural Materials in Reactor Technology (SMIRT 13), Porto Alegre, Brazil, August 13–18, Division E, Universidade Federal do Rio Grande du Sul (UFRGS), 1995, p. 563.
[14] A.-A.F. Tavassoli, RAFM steels – rules for design and inspection, Annual report of the Association Euratom/CEA (2000) 235.
[15] K. Shiba, Report of JAERI-Tech-97-038, JAERI-1998, Tokyo, Japan.
[16] R.L. Klueh, D.S. Gelles, S. Jitsukawa, A. Kimura, G.R. Odette, B. van der Schaaf, M. Victoria, 10th International Conference on Fusion Reactor Materials, Baden-Baden, Germany, October 14–19, 2001.
[17] S. Ukai, S. Mizuta, T. Yoshitake, T. Okuda, M. Fujiwara, S. Hagi, T. Kobayashi, J. Nucl. Mater. 283–287 (2000) 702.
[18] S. Revol, S. Launois, R. Baccino, G. Le Marois, SOFT 2000.
[19] A. Alamo, H. Regle, G. Pons, L.L. Bechade, Mater. Sci. Forum 88–90 (1992) 183.
[20] D.K. Mukhopadhyay, F.H. Froes, D.S. Gelles, J. Nucl. Mater. 258–263 (1998) 1209.
[21] D. Smith, M.C. Billone, K. Natesan, Vanadium-base alloys for fusion first-wall/blanket applications, in: Ninth International Conference on Fusion Reactor Materials, Colorado Springs, CO, October 10–15, 1998.
[22] M.C. Billone, in: Fusion Materials Semiann. Prog. Report for period ending December 31, 1997, DOE/ER-0313/23, Oak Ridge National Lab, 1997, p. 3.
[23] A.N. Gubbi, A.F. Rowcliffe, W.S. Eatherly, L.T. Gibson, in: Fusion Materials Semiannual Progress Report for Period ending June 30, 1996, DOE/ER-0313/20, Oak Ridge National Lab, 1996, p. 38.
[24] E.V. van Osch, M.I. de Vries, J. Nucl. Mater. 258–263 (1998) 301.
[25] S.J. Zinkle, A.F. Rowcliffe, C.O. Stevens, in: Fusion Materials Semiann. Prog. Report for period ending June 30, 1998, DOE/ER-0313/24, Oak Ridge National Lab, 1998, p. 1.
[26] K.C. Liu, J. Nucl. Mater. 103&104 (1981) 913.
[27] B.G. Gieseke, C.O. Stevens, M. Grossbeck, J. Nucl. Mater. 233–237 (1996) 488.
[28] W. van Wizenburg, H.J. de Bruyne, ASTM STP 1175, Ph. 1993.
[29] S.J. Zinkle, Thermo-physical and mechanical properties of V–(4–5%)Cr–(4–5%)Ti alloys, in: Fusion Materials Semiann. Prog. Report for period ending December 31, 1997, DOE/ER-0313/23, Oak Ridge National Lab, 1997, p. 99 (updated mid-1998).
[30] M. Satou, H. Koide, A. Hasegawa, K. Abe, H. Kayano, H. Matsui, J. Nucl. Mater. 233–237 (1996) 447.
[31] E.V. van Osch (Ed.), Report of the Second IEA Workshop on vanadium alloy development for fusion, ECN-R-96-012, Netherlands Energy Research Foundation ECN, 1996, p. 417.
[32] H. Tsai, L.J. Nowicki, M.C. Billone, H.M. Chung, D.L. Smith, in: Fusion Materials Semiann. Prog. Report for period ending December 31, 1997, DOE/ER-0313/23, Oak Ridge National Lab, 1997, p. 70.
[33] S.J. Zinkle, H. Matsui, D.L. Smith, A.F. Rowcliffe, E. van Osch, K. Abe, V.A. Kazakov, J. Nucl. Mater. 258–263 (1998) 205.
[34] R. Wadsack, R. Pippan, B. Schedler, 10th International Conference on Fusion Reactor Materials, October 14–19, Baden-Baden, Germany, 2001.

[35] S.J. Zinkle, L.L. Snead, Thermo-physical and mechanical properties of SiC/SiC composites, in: Fusion Materials Semiann. Prog. Report for period ending June 30, 1998, DOE/ER-0313/24, Oak Ridge National Lab, 1998, p. 93.
[36] M. Takeda, J. Sakamoto, A. Saeki, H. Ichikawa, in: Ceramic Engineering and Science Proceedings, vol. 17, no. 4, American Ceramic Society, Westerville, OH, 1996, p. 35.
[37] J. Lipowitz, J.A. Rabe, A. Zangvil, Y. Xu, in: Ceramic Engineering and Science Proceedings, vol. 18, no. 3, American Ceramic Society, Westerville, OH, 1997, p. 147.
[38] M.C. Osborne, PhD thesis, Department of Materials Science and Engineering, Rensselaer Polytechnic Institute, 1997.
[39] G.E. Youngblood, R.H. Jones, G.N. Morscher, A. Kohyama, in: Fusion Materials Semiann. Prog. Report for period ending June 30, 1997, DOE/ER-0313/22, Oak Ridge National Lab, 1997, p. 81.
[40] R.H. Jones, D. Steiner, H.L. Henisch, G.A. Newsome, H.M. Kerch, J. Nucl. Mater. 245 (1997) 87.
[41] E. Lara-Curzio, Properties of CVD Ceramic Matrix Composites, Comprehensive Composite Materials Encyclopedia, Vol. 4, Ch. 18, Elsevier, London, August 2000.
[42] C.A. Lewinsohn, M.L. Hamilton, G.E. Youngblood, R.H. Jones, F. Garner, S.L. Hecht, A. Kohyama, J. Nucl. Mater. 253 (1998) 36.
[43] Z. Zhu, P. Jung, J. Nucl. Mater. 212–215 (1994) 1081.
[44] H. Golfier, G. Aiello, R. Coutourier, M. Fütterer, L. Giancarli, A. Li Puma, Y. Poitevin, J.F. Salavy, J. Szczepanski, Progress on the TAURO Blanket System, to be presented at the ISFNT-6, April 7–13, 2002, San Diego, CA.
[45] D.J. Senor, D.J. Trimble, G.A. Newsome, J.J. Woods, Ceramic Engineering and Science Proceedings, vol. 18, no. 3, American Ceramic Society, Westerville, OH, 1997, p. 591.
[46] R.H. Jones, L. Giancarli, A. Haegawa, Y. Katoh, A. Kohyama, B. Riccardi, L.L. Snead, W.J. Weber, 10th International Conference on Fusion Reactor Materials, Baden-Baden, Germany, October 14–19, 2001.
[47] D.J. Senor et al., Fusion Technol. 30 (1996) 943.
[48] L.L. Snead, R.H. Jones, A. Kohyama, P. Fenici, J. Nucl. Mater. 233–237 (1996) 26.
[49] R.H. Jones, C.H. Henager Jr., G.E. Youngblood, H.L. Heinisch, Fusion Technol. 30 (1996) 969.
[50] L.L. Snead, M.C. Osborne, R.C. Lowden, J. Strizak, R.J. Shinavski, K.L. More, W.S. Eatherly, J. Bailey, A.M. Williams, J. Nucl. Mater. 253 (1998) 20.
[51] M.C. Osborne, C.R. Hubbard, L.L. Snead, D. Steiner, J. Nucl. Mater. 253 (1998) 67.
[52] D.J. Senor, G.E. Youngblood, C.E. Moore, D.J. Trimble, G.A. Newsome, J.J. Woods, Fusion Technol. 30 (1996) 943.
[53] G.W. Hollenberg et al., J. Nucl. Mater. 219 (1995) 70.
[54] R. Blackstone, E.H. Voice, J. Nucl. Mater. 39 (1971) 319.
[55] R. Price, Nucl. Technol. 35 (1977) 320.
[56] L.L. Snead, S.J. Zinkle, J.C. Hay, M.C. Osborne, Nucl. Instrum. Meth. B 141 (1998) 123.
[57] A.-A.F. Tavassoli, Met Trans. 2 (1971) 1985.
[58] A.-A.F. Tavassoli, Welding J. 4 (1973) 168s.
[59] A.-A.F. Tavassoli, Welding J. 7 (1973) 323S.
[60] S.J. Zinkle, Thermo-physical and mechanical properties of Ta–8% W–2% Hf alloys, in: Fusion Materials Semiann. Prog. Report for period ending December 31, 1999, DOE/ER-0313/27, Oak Ridge National Lab, 1999, p. 175.
[61] A.-A.F. Tavassoli, B. Vrillon, G. Robert, Design and Evaluation of Materials for Space Reactors, in: L.H. Larsson (Ed.), High Temperature Structural Design, International Conference Venice, 24–26 October 90, EISS12, Mechanical Eng., London, 1992, p. 127.
[62] M. Scibetta, R. Chaouadi, J.L. Puzzolante, J. Nucl. Mater. 283–287 (2000) 455.
[63] A. Hasegawa, K. Ueda, M. Satou, K. Abe, J. Nucl. Mater. 258–263 (1998) 902.
[64] J.M. Steichen, J. Nucl. Mater. 60 (1976) 13.
[65] V. Chakin, V. Kazakov, J. Nucl. Mater. 233–237 (1996) 570.
[66] S.A. Fabritsiev, A.S. Pokrovsky, J. Nucl. Mater. 252 (1998) 216.
[67] K.A. Faymon, J.S. Fordyce, Space Power Technology into the 21st Century, NASA TM 83690, Lewis Research Center, Cleaveland, OH, 1984.
[68] K.M. Leisner, SP-100 powers for space based radars, American Institute of Aeronautics and Astronautics, 1987.
[69] S.J. Zinkle, Thermo-physical and mechanical properties of Ta–8% W–2% Hf alloys, in: Fusion Materials Semiann. Prog. Report for period ending December. 31 1999, DOE/ER-0313/27, Oak Ridge National Lab, 1999, p. 175.
[70] R.W. Buckman Jr., in: High Temperature Silicides and Refractory Alloys, in: C.L. Briant et al. (Eds.), MRS Symposium Proceedings, vol. 322, Materials Research Society, Pittsburgh, 1994, p. 329.
[71] D.C. Goldberg, in: W.F. Brown Jr. (Ed.), Aerospace Structural Metals Handbook, AFML-TR 68-115, Metals and Ceramics Information Center, Battelle Columbus Laboratories, 1969.
[72] T.E. Tietz, J.W. Wilson, Behavior and Properties of Refractory Metals, Stanford University, Stanford, CA, 1965.
[73] F.W. Wiffen, in: R.J. Arsenault (Ed.), Proceedings of the International Conference on Defects and Defect Clusters in BCC Metals and Their Alloys, Nuclear Metallurgy, vol. 18, National Bureau of Standards, Gaithersburg, MD, 1973, p. 176.
[74] H.E. McCoy, Oak Ridge National Lab Report ORNL/TM-10127 (1986).
[75] J.B. Conway, in: R.H. Cooper Jr., E.E. Hoffman (Eds.), Proceedings of the Symposium on Refractory Alloy Technology for Space Nuclear Power Applications, CONF-8308130, Oak Ridge National Lab, 1984, p. 252.
[76] K.D. Sheffler, J.C. Sawyer, E.A. Steigerwald, Trans. Am. Soc. Met. 62 (1969) 749.
[77] J.R. Hughes, in: High Temperature Silicides and Refractory Alloys, in: C.L. Briant et al. (Eds.), MRS Symposium Proceedings, vol. 322, Materials Research Society, Pittsburgh, PA, 1994, p. 363.
[78] J.H. DeVan, J.R. DiStefano, E.E. Hoffman, in: R.H. Cooper Jr., E.E. Hoffman (Eds.), Proceedings of the Symposium on Refractory Alloy Technology for Space Nuclear Power Applications, CONF-8308130, Oak Ridge National Lab, 1984, p. 34.
[79] J.R. DiStefano, J. Mater. Eng. 11 (1989) 215.

[80] E.E. Hoffman, J.H. DeVan, J.R. DiStefano, in: E.N.C. Dalder, T. Grobstein, C.S. Olsen (Eds.), Evolution of Refractory Metals and Alloys, The Minerals, Metals and Materials Society, Warrendale, PA, 1994, p. 137.
[81] R.H. Burns, F.S. Shuker Jr., P.E. Manning, in: R.E. Smallwood (Ed.), Refractory Metals and Their Industrial Applications, ASTM STP 849, American Society for Testing and Materials, Philadelphia, PA, 1984, p. 50.
[82] C.W. Marshall, F.C. Holden, Fracture toughness of refractory metals and alloys, in: R.W. Fountain et al. (Eds.), High Temperature Refractory Metals: Metallurgical Society Conference 34, Gordon and Breach, New York, 1966, p. 129.
[83] A.V. Babak, E.I. Uskov, Strength Mater 16 (1984) 943.
[84] Y.N. Podrezov, O.G. Radchenko, N.G. Danilenko, V.V. Panichkina, V.I. Gachegov, O.B. Ol'shanskii, Sov. Powder Metall. Metal Ceram. 26 (1987) 677.
[85] Y. Mutoh, K. Ichikawa, K. Nagata, M. Takeuchi, J. Mater. Sci. 30 (1995) 770.
[86] P. Gumbsch, J. Riedle, A. Hartmaier, H.F. Fischmeister, Science 282 (1998) 1293.
[87] V.R. Barabash, in ITER Materials Assessment Report, ITER Document No. G A1 DDD 01 97-08-13 W0.1, 1998..
[88] F.W. Wiffen, Effects of irradiation on properties of refractory alloys with emphasis on space power reactor applications, in: R.H. Cooper Jr., E.E. Hoffman (Eds.), Proceedings of the Symposium on Refractory Alloy Technology for Space Nuclear Power Applications, CONF-8308130, Oak Ridge National Lab, 1984, p. 252.
[89] V. Chakin, V. Kazakov, J. Nucl. Mater. 233–237 (1996) 570.
[90] P. Krautwasser, H. Derz, E. Kny, High Temp.–High Press. 22 (1976) 25.